 doi:10.20944/preprints202012.0157.v1

Research Article

Title: 3D bioprinted material that recapitulates the perivascular bone marrow structure for sustained hematopoietic and cancer models.

Authors: Caitlyn A. Moore [1,2], Zain Siddiqui [3], Griffin J. Carney [1], Yahaira Naaldijk [1], Khadidiatou Guiro [1], Murat Guvendiren [3,4], Vivek A. Kumar [3,4,5], Pranela Rameshwar [1*]

[b]Department of Medicine, Rutgers New Jersey Medical School, Newark, NJ, USA 07103

[2] Rutgers School of Graduate Studies, New Jersey Medical School, Newark, NJ, USA 07103

[3] Department of Biomedical Engineering, New Jersey Institute of Technology, 323 Martin Luther King Jr. Blvd, Newark, NJ, USA 07102

[4] Department of Chemical, Biological and Pharmaceutical Engineering, New Jersey Institute of Technology, 323 Martin Luther King Jr. Blvd, Newark, NJ, USA 07102

[5] Department of Restorative Dentistry, Rutgers School of Dental Medicine, 110 Bergen St, Newark, NJ, USA 07103

*__Corresponding Author__: Pranela Rameshwar, Rutgers New Jersey Medical School, 185 South Orange Avenue, Newark, NJ 07103. Email: rameshwa@njms.rutgers.edu

 doi:10.20944/preprints202012.0157.v1

Abstract

Translational medicine requires facile experimental systems to replicate the dynamic biological systems of diseases. Drug approval continues to lag, partly due to incongruencies in the research pipeline that traditionally involve 2D models, which could be improved with 3D models. The bone marrow (BM) poses challenges to harvest as an intact organ making it difficult to study disease processes such as breast cancer (BC) survival in BM, and to effective evaluation of drug response in BM. Furthermore, it is a challenge to develop 3D BM structures due to its weak physical properties, and complex hierarchical structure and cellular landscape. To address this, we leveraged 3D bioprinting to create a BM structure with varied methylcellulose (M):alginate (A) ratios. We selected hydrogels containing 4% (w/v) M and 2% (w/v) A, which recapitulates rheological and ultrastructural features of the BM while maintaining stability in culture. This hydrogel sustained the culture of two key primary BM microenvironmental cells found at the perivascular region, mesenchymal stem cells and endothelial cells. More importantly, the scaffold showed evidence of cell autonomous dedifferentiation of BC cells to cancer stem cell properties. This scaffold could be the platform to create BM models for various disease and also for drug screening.

Keywords: Alginate, methylcellulose, hydrogel, bone marrow, bioprinting, breast cancer, stem cells

 doi:10.20944/preprints202012.0157.v1

1. Introduction

Translational medicine is propelled by a cyclical bench-to-bedside-to-bench approach in which laboratory data drives clinical strategies, generating questions for further investigation in the lab. However, this iterative process is largely driven by two-dimensional (2D) *in vitro* and/or preclinical animal models, which alone may not be sufficient for effective translation to the clinical arena. The reports indicated drug approval rate by the US Food and Drug Administration (FDA) hovers around 10%, with ~54% failure during late-stage clinical development. This has been largely attributed to "inadequate efficacy" [1-3] . Together, these findings indicate that research and development approaches must evolve in order to improve translation efficiency.

The incorporation of three-dimensional (3D) *in vitro* cell culture platforms into translational research has allowed investigators to improve on evaluating the role of the microenvironment on cell behavior and fate, in addition to providing a more physiologically relevant culture system to vet the efficacy of therapeutics [4, 5]. In recent years, 3D bioprinting has emerged as a particularly powerful technique to create highly specialized and customizable 3D *in vitro* systems for the purposes of tissue modeling and regeneration [6]. To this end, 3D bioprinting has led to the successful development of *de novo* tissues and organs that are phenotypically and functionally similar to their natural counterparts [7-12].

Bone marrow (BM) is a primary lymphoid organ and the site of hematopoiesis, which produced blood and immune cells throughout life. The BM is a complicated organ to replicate *in vitro* because it is a pliant, gelatinous tissue containing densely packed heterogeneous cells [13-18]. The development of biomimetic 3D *in vitro* BM models is critical for a variety of reasons. First, hematological malignancies represent approximately 10% of new cancer diagnoses annually in the US, and based on current data, only an estimated 26% of the drugs in development for these

 doi:10.20944/preprints202012.0157.v1

conditions will obtain FDA approval [2, 19] . Second, the role of the BM microenvironment in healthy and dysfunctional hematopoiesis has become more well-defined in recent years; reports have shown that cell composition and distribution, tissue structure, and other biological and physical factors govern the fate of hematopoiesis [20, 21]. Importantly, BM also supports both hematologic and non-hematologic malignancies. As a result, the BM has been identified as a source of cancer relapse and progression [22-26]. Moreover, for approval of cancer drugs by the FDA, the drug must show direct evidence of clinical benefit or improvement with a surrogate endpoint. The latter could be improvement in overall survival, quality of life, and/or physical functioning [27]. Hematopoietic function runs hand-in-hand with such metrics, underpinning the importance of evaluating the effect of drugs and their dosage on BM cells [28, 29].

In order to unlock the vast capabilities of 3D bioprinting for *in vitro* BM model development, it is imperative to design a hydrogel-based bioink amenable to extrusion that also sufficiently recapitulates the microenvironment. Although hydrogels are often used to mimic soft tissues, it is challenging to bioprint self-supporting mechanically-stable hydrogels with an elastic modulus below 1 kPa [30, 31]. Informed by our experience with hematopoietic cell culture and bioinks previously reported in the literature, we created a bioink comprised of methylcellulose (MC) and alginate. MC is a thermally-gelling polymer widely used as a binder, thickener, or emulsifier in industrial applications, but is gaining popularity for its value in biomedical applications, including drug delivery and cell culture [32-36]. Alginate, similarly, is a frequently used material for bioink development due to its rapid ion dependent crosslinking and shear thinning behavior [37, 38].

In this study, MC-alginate hydrogel bioinks were fabricated according to the well-established use of MC matrices to study hematopoietic progenitors in colony forming assays. After

Preprints (www.preprints.org) | NOT PEER-REVIEWED | Posted: 7 December 2020 doi:10.20944/preprints202012.0157.v1

in-depth characterization and evaluation, we determined 2 of the initial 9 hydrogel formulations demonstrated properties aligned with both extrusion bioprinting and BM modeling: 4% (w/v) MC and 2% (w/v) alginate (4:2), and 6% (w/v) MC and 2% alginate (6:2). We purport that 4:2 bioink, in particular, more closely replicates select properties of BM than 6:2 bioink, such as gross architecture, availability of oxygen, and rheological characteristics. The bioinks reported in this study may serve as a foundational tool to model different BM microenvironment through desired cellular printing and also by tagging specific molecules to the scaffold that could facilitate cell adhesion, and release of soluble factors. We anticipate that 4:2 bioink will serve as a conduit between 2D *in vitro* and pre-clinical animal models to enhance the efficacy of translating the science and to improve on drug screening. These fundamental improvements may serve the critical gap between 2D *in vitro* and pre-clinical animal models, consequently to impact quality of life and survival.

2. Materials and Methods

2.1 Ethics Statement

BM mesenchymal stem cells (MSCs) and endothelial cells (ECs) were isolated from BM aspirates from healthy subjects between 18 and 35 years as described below. The Institutional Review Board of Rutgers, Newark, NJ, approved the protocol. All subjects provided informed consent.

2.2 Reagents

Alginic acid sodium salt (alginate), 4000 cPs methylcellulose (MC), and phosphate-buffered saline (PBS) without Ca^{2+} and Mg^{2+}, Accutase cell dissociation reagent, alginate lyase (alginase), Ficoll Hypaque, $ZnCl_2$, KI, and I_2 were purchased from Sigma-Aldrich (St. Louis MO). Iscove's Modified Eagle Medium (IMEM), Dulbecco's Modified Eagle Medium (DMEM), PBS with Ca^{2+} and Mg^{2+}, and tissue culture grade liquid 7.5% sodium bicarbonate, and 1X insulin-transferrin-

Preprints (www.preprints.org) | NOT PEER-REVIEWED | Posted: 7 December 2020 doi:10.20944/preprints202012.0157.v1

selenium were purchased from Gibco (Grand Island NY). L-glutamine (LG), Penicillin-Streptomycin (PS), and fetal bovine serum (FBS) were purchased from ThermoFisher Scientific (Waltham MA). EGM-2 Endothelial Growth Media was purchased from Lonza (Walkersville MD). Lox-1 Hypoxia Probe was purchased from Organogenix (Kanagawa Japan). G418 sulfate solution was purchased from Gemini Bio-Products (West Sacramento CA). Extra-pure calcium chloride dihydrate crystals were purchased from EM Science (Gibbstown NJ). Hoechst-33342, rhodamine phalloidin, DAPI, C_{12} Resazurin, and SYTOX Green were purchased from Invitrogen (Eugene OR).

2.3 Bioink fabrication

Sterile (autoclaved) alginate was mixed to homogeneity in 60°C deionized water (dH_2O). Following this, we slowly added sterile (autoclaved) MC with constant mixing. The suspension was equilibrated to room temperature through addition of chilled dH_2O. This was followed by addition of IMEM and sodium bicarbonate with mixing to homogeneity at room temperature. The mixture was transferred to 4°C for 1 hour to facilitate gelation. Bioinks were aliquoted and kept at 4°C or -20°C for short- or long-term storage, respectively. Prior to printing, the active bioink aliquots were brought to room temperature.

2.4 Rheological analyses

Rheological tests were performed using a DHR-2 Rheometer (TA Instruments, New Castle DE) as described. Briefly, bioinks were plated on a 40-mm parallel Peltier plate geometry (gap width: 1000 um). Strain sweep (0.1-100% strain, at 2 Hz) and shear recovery (0.1% strain for 1 min followed by 4 repetitions of 100% strain for 1 min and 0.1% strain for 5 min) tests were performed at room temperature.

Preprints (www.preprints.org) | NOT PEER-REVIEWED | Posted: 7 December 2020 doi:10.20944/preprints202012.0157.v1

2.5 Fidelity

The Rutgers University 'R' logos were printed on Parafilm. Constructs were photographed immediately following printing. Five distinct dimensions of constructs were measured using ImageJ (NIH, Bethesda MD) and compared to same dimensions of the CAD-designated geometry. The dimension differences were dimensions was calculated by dividing the dimension of the printed construct by the CAD-designated dimension (printed/CAD).

2.6 Bioprinting

All model creation and bioprinting was performed using CELLINK® INKREDIBLE 3D Bioprinter (CELLINK AB, Sweden). A 22G polypropylene nozzle (CELLINK AB, Sweden) was used for printing all structures. Briefly, cell-free bioink (for cell-laden bioink, refer to "Preparation of cell-laden scaffolds" section below) was loaded into the printer cartridge with attached nozzle. Then, bioprinter X-Y-Z axes were calibrated, printing pressure was adjusted to ensure continuous flow, and scaffolds were printed. Assays described in the following sections used 4-layer lattice cubic scaffolds (6-mm x 6-mm x 1.2-mm) in 24-well plates (TPP, Switzerland) unless otherwise noted. After bioprinting, scaffolds were crosslinked with sterile 100 mM $CaCl_2$ solution for 5-10 mins, washed with the appropriate culture solution for 20 mins to remove excess $CaCl_2$ and incubated in standard culture conditions (37°C, 5% CO_2, and 95% relative humidity).

2.7 Bone marrow aspirate and cell isolation

Bone marrow (BM) mononuclear cells (MNCs), mesenchymal stem cells (MSCs), and endothelial cells (ECs) were isolated from BM aspirates from posterior iliac crests of healthy subjects between 18 and 35 yrs. The use of human BM aspirates followed an protocol, approved by the Institutional Review Board of Rutgers.

Preprints (www.preprints.org) | NOT PEER-REVIEWED | Posted: 7 December 2020 doi:10.20944/preprints202012.0157.v1

2.8 Bone marrow (BM) mesenchymal stem cell culture

MSC culture used BM aspirate and the method was previously described [39, 40]. Briefly, unfractionated BM aspirates were diluted in DMEM containing 10% FBS and then seeded in plasma-treated Falcon 3003 Petri dishes. The plates were incubated at 37°C, 5% CO_2, and 95% relative humidity. After 72 h, the MNCs were selected by Ficoll Hypaque density gradient centrifugation and re-plated on the dishes with 10% DMEM. Media was partially changed twice weekly. At 80% confluence, the adherent cells were subjected to serial passages. At passage 5, the cells were $CD45^-$, $CD14^-$, $CD44^+$, $CD29^+$, $CD105^+$, and $CD34^-$.

2.9 BM endothelial cell culture

MNCs were isolated from unfractionated BM aspirates by Ficoll Hypaque density gradient centrifugation as described in the previous section. MNCs were subsequently seeded in T25 tissue culture flasks (Greiner Bio-One, Monroe NC) at a density of 10^7 with EGM-2 Endothelial Growth Media for up to 21 days. At confluence, the adherent cells are subjected to serial passages.

2.10 Preparation of cell-laden scaffolds

Cells were dissociated using Accutase and resuspended in 150 µl of media for mixing with bioink. Cells were mixed into 4:2 or 6:2 bioink using two Luer lock adapter-connected 3 ml syringes at a density of $1x10^6$ cells/ml bioink. Cell-laden bioinks were loaded into cartridges, printed, and crosslinked with sterile 100 mM $CaCl_2$ for 5-10 minutes. Scaffolds were then washed for 20 mins in the appropriate culture solution and incubated in standard culture conditions (37°C, 5% CO_2, and 95% relative humidity).

2.11 Cell viability and vitality

LIVE/DEAD Cell Vitality Assay Kit (Invitrogen) assessed cell health, according to manufacturer instructions. Healthy living cells were stained red (C_{12} Resazurin), injured living cells were stained

Preprints (www.preprints.org) | NOT PEER-REVIEWED | Posted: 7 December 2020 doi:10.20944/preprints202012.0157.v1

yellow or orange (C_{12} Resazurin + SYTOX Green), and dead cells were stained green (SYTOX Green). Images were acquired with the Fluoview FV10i Confocal Microscope (Olympus, Tokyo Japan). Each time point include images from 8 technical and 4 biological replicates. The images were analyzed with FV10-ASW Viewer Software (Olympus) and ImageJ.

2.12 Cell morphology

Scaffolds were fixed with a solution of 90% methanol and 10% acetic acid for at least 20 mins. Fixed scaffolds were washed twice with PBS without Ca^{2+} and Mg^{2+} and stained. Scaffolds containing MSCs and ECs were stained with DAPI and rhodamine phalloidin. Images were acquired using a Fluoview FV10i Confocal Microscope. Images were analyzed using FV10-ASW Viewer Software and ImageJ.

2.13 Scanning electron microscopy

4:2 and 6:2 cell-free scaffolds were printed, crosslinked, and cultured for 72 h in 10% FBS DMEM containing 1% (v/v) LG and 1% (v/v) PS before being processed for scanning electron microscopy (SEM) as described. Briefly, scaffolds were fixed with glutaraldehyde, dehydrated via exchange with ethanol, and critical point dried. Dehydrated scaffolds were viewed using JSM-7900F Schottky Field Emission Scanning Electron Microscope (JEOL USA, Inc., Peabody MA) with an accelerating voltage of 2-3 kV.

2.14 Hypoxia assessment

4:2 and 6:2 bioink cell-laden scaffolds were treated with 2 µM Lox-1 Hypoxia Probe at 48 h after printing. The scaffolds were incubated and after 24 h they were imaged with the Fluoview FV10i Confocal Microscope. Bothe “Normoxic and hypoxic incubation” used standard culture conditions (37°C, 5% CO_2, 95% relative humidity). However hypoxic conditions used parafilm sealed plates, which impeded gas exchange with the ambient environment. The presence or absence of red

Preprints (www.preprints.org) | NOT PEER-REVIEWED | Posted: 7 December 2020 doi:10.20944/preprints202012.0157.v1

fluorescence of the Lox-1 probe was quantified using FV10-ASW Viewer Software and ImageJ.

2.15 Scaffold degradation assessment

4:2 and 6:2 cell-free scaffolds were cultured in 1 of 6 culture solutions: DMEM containing 1% (v/v) LG, 1% (v/v) PS, and either 10%, 2%, or 0% FBS, PBS with and without Ca^{2+} and Mg^{2+}, and ultrapure dH_2O. DMEM with 0% FBS was supplemented with 1X insulin-transferrin-selenium as would occur when printing cell-laden scaffolds. Scaffolds were photographed immediately following crosslinking (Week 0) followed by weekly intervals up to 12 weeks for observable degradation (e.g. loss of shape, fractionation). At the same weekly intervals, culture solutions were collected to measure free MC and Ca^{2+} as indicators of long-term MC elution and Ca^{2+}-mediated alginate crosslink breakage, respectively, as described.

2.16 Methylcellulose release analyses

4:2 and 6:2 cell-free scaffolds were printed and cultured in the 6 aforementioned culture solutions. Culture solutions were collected weekly for 12 wks. All collected samples were stored in 1.5 ml centrifuge tubes at 4°C until time of assay. A colorimetric assay was developed to quantify MC concentration in each solution. Briefly, 150 µl was added to a 96-well plate. 50 µl of chlorine-zinc-iodine (Cl-Zn-I) solution was added to each well to stain MC [41]. After addition of stain, plates were gently agitated for 5-10 minutes. Absorbance was measured using a microplate reader at 500 nm [42]. MC concentration was calculated based on a standard curve of 0.001 to 1% (w/v) aqueous MC. Concentrations are reported in µg/µl.

Cl-Zn-I solution followed a previously described protocol [41]. Briefly, 50 g of $ZnCl_2$ was thoroughly mixed in 25 ml dH_2O. In a separate solution, 5 g KI and 0.25 g I_2 were added to 125 ml dH_2O and mixed thoroughly. This was followed by combining the $ZnCl_2$ aqueous solution to KI-I_2 solution. The final solution was stored in a glass bottle at room temperature.

Preprints (www.preprints.org) | NOT PEER-REVIEWED | Posted: 7 December 2020 doi:10.20944/preprints202012.0157.v1

2.17 Ca^{2+}-mediated alginate crosslink breakage analyses

4:2 and 6:2 cell-free scaffolds were printed and cultured in1 of the 6 aforementioned culture solutions. Culture solutions were collected weekly for 12 wks. All collected samples were stored in 1.5 ml centrifuge tubes at 4°C until time of assay. Concentration of Ca^{2+} in each sample was determined a Calcium Colorimetric Assay Kit (Sigma-Aldrich, St. Louis MO) according to manufacturer instructions. Briefly, 50 µl of each sample was added to a 96-well plate with Chromogenic Reagent and Assay Buffer. Plates were gently agitated in the dark for 5-10 mins. Absorbance was measured using a microplate reader at 570 and 600 nm. Ca^{2+} concentrations are reported in µg/µl.

2.18 Scaffold weight fluctuation measurements

4:2 and 6:2 cell-free scaffolds were printed and cultured in 1 of the 6 aforementioned culture solutions. The base line scaffold weight was determined immediately following crosslinking (W_0) and subsequent weights at 5, 30, and 90 min, and 1, 3, 7, 10, and 14 days post-printing (W_x). Weight change ratio (W_x/W_0), indicating scaffold swelling or shrinkage, was calculated at each time point for each solution and compared to baseline (W_0/W_0).

2.19 Cell Line

MDA-MB-231 (highly invasive, basal-like) triple negative (TN) breast cancer cells (BCCs) were purchased from American Type Culture Collection (ATCC) and cultured per manufacturer's instructions. The BCCs were stably transfected with pEGFP1-Oct3/4 as described [43]. Stable transfectants were maintained with G418 (50 mg/µl). The cells were authenticated with ATCC STR database (www.atcc.org/STR_database.aspx). Cells were also screened weekly for Mycoplasma.

Preprints (www.preprints.org) | NOT PEER-REVIEWED | Posted: 7 December 2020 doi:10.20944/preprints202012.0157.v1

2.20 Sorting of BCC subsets

BCC subsets were selected as described [43]. Briefly, MDA-MB-231 with stable pOct4a-GFP were sorted, based on GFP intensity on the FACSDiva fluorescence-assisted cell sorter (FACS) (BD Biosciences, San Jose CA). Oct4a-GFP^{high} (top 5% intensity), Oct4a-GFP^{med} (middle 20%), and Oct4a-GFP^{low} (bottom 5%) subsets were sorted, as described [44]. The Oct4a-GFP^{high} population has been previously shown to be tumor-initiating and have self-renewal properties and will be referred to herein as cancer stem cells (CSCs) [43].

2.21 Statistical Analysis

Student's t-test compared differences between data points with Kruskal-Wallis post-hoc analysis unless otherwise stated. *P* values <0.05 were considered statistically significant. Images from the cell health analyses were determine via 2-way ANOVA.

3 **Results**

3.1 Selection of bioink formulations

In order to recapitulate the BM microenvironment with 3D bioprinting, it is important to establish a bioink that maintains printability and stability. Thus, we created and characterized 9 bioinks with varied concentrations of MC and/or alginate. We designated the bioink formulations based on the MC:alginate concentration (i.e., 1:2 = 1% [w/v] MC and 2% [w/v] alginate). Bioinks were scored and evaluated according to 4 objectively weighted criteria within a decision matrix: Ease of Fabrication (15%), Fidelity (20%), Handleability (30%), and Extrudability (35%) (Table S1). Results of the decision matrix identified 2 of the highest scored 9 bioinks for further study: 4% MC and 2% alginate (4:2) and 6% MC and 2% alginate (6:2).

3.2 Rheometric analyses of bioinks - similarity to BM tissue

Rheometric analyses to assess the mechanical behavior of the bioinks indicated that the

 doi:10.20944/preprints202012.0157.v1

concentration of MC was proportional to the viscosity and indirectly proportional to flow capacity (Figures 1 A-F). We observed that increasing the MC concentration of the hydrogel by 2% (w/v) resulted in an order of magnitude increased viscosity and shear stress required for flow (Figures 1A-F). Additionally, bioinks exhibited shear-thinning behavior that closely correlated to the concentration of alginate in the hydrogel (Figures 1A-C). Shear thinning is advantageous for extrudability of bioinks and preservation of cell integrity, as well as mimicry of BM tissue architecture [15, 16, 45]. Importantly, rheological analyses showed similar flow properties to that of human BM tissue, reported by Sobotková and colleagues (Figure1G).

The fidelity of bioprinted structures depends on the ability of a bioink to shear recover following extrusion. In addition to the order of magnitude increase in viscosity per 2% increase in concentration of MC, we observed a similar increase in the shear modulus, or G′, of the hydrogels (Figures 1H-J). It should be noted that G′ for 4:2 and 6:2 bioinks are comparable to bioinks of similar composition and fall within the range of those reported for BM tissue [15, 17, 46-49]. In shear recovery studies, it was observed that 4:2 and 6:2 bioinks were able to reach pre-shear G' during the 5-minute recovery period at low shear (0.01%), a behavior that was also demonstrated by hydrogels comprised of equivalent concentrations of MC or alginate (Figures 1H-J). However, full recovery of the 4:2 and 6:2 bioinks required the 5-minute recovery period when they approached their pre-shear G' (~9x% recovery) as compared to the equivalent single-component hydrogels, which recovered almost immediately (Figures 1H-J).

We corroborated shape fidelity by analyzing the rheological properties of hydrogels (Figure 1K). The indicated bioinks tested with 2% MC or less were unable to achieve or maintain the designated structure due to their low viscosity and elastic modulus (Figure 1L). However, those with 4% MC or 6% MC were able to achieve and maintain the designated structure with varying

Preprints (www.preprints.org) | NOT PEER-REVIEWED | Posted: 7 December 2020 doi:10.20944/preprints202012.0157.v1

degrees of success (Figure 1L).

Although 4% MC bioinks were less viscous than 6% MC bioinks, 4:0 bioink did not extrude well. Rather, the resulting constructs appear as incomplete structures in some of the areas. In contrast, the 4:1 and 4:2 bioinks were extruded relatively easy due to their enriched shear thinning behavior, but still showed spreading that may be attributable to slow shear recovery. Altogether, the selected 4:2 and 6:2 bioinks (Table S1) showed rheological similarities to native BM tissue. Although, the 4:2 bioink was more representative of BM elastic modulus and flow properties.

We compared the mechanical properties of our bioprinted scaffolds alongside a spectrum of elastic moduli (G′) of various bodily tissues and biomaterials, based on the literature (Figure 1M). Femur generally falls within a broad range between 100 Pa and 100 kPa. However, the marrow/inner material is located below 1 kPa because the perivascular and central niches fall on the low end of this range. As noted in the diagram, the 3D structures with 4:2 with methylcellulose-alginate bioink has shown similarities with respect to the mechanical property of the marrow.

3.3 Cell health following extrusion

The utility of 3D bioprinting is partly derived from the ability to print cell-embedded scaffolds [50]. Thus, it is crucial to evaluate the effect of extrusion on health of the printed cells using the selected 4:2 and 6:2 bioinks and two primary human BM niche cells, mesenchymal stem cells (MSCs) and endothelial cells (ECs). The cells were printed using 25 kPa pressure into cubic scaffolds (dimensions: 6 mm x 6 mm x 1.2 mm) and evaluated after 7 days of culture using the Live/Dead cell vitality assay. The assay is based on the reduction of C12-resazurin to red-fluorescent C12-resorufin when cells are metabolically active. The dead cells such as those in late apoptosis and necrotic will uptake SYTOX® Green dye, resulting in total demarcation of

 doi:10.20944/preprints202012.0157.v1

metabolically active and dead cells.

The data indicated that approximately half of MSCs and ECs printed in both 4:2 and 6:2 bioinks showed reduced resorufin indicating some form of membrane injury during extrusion (Figures 2A-D). However, since the presence of resorufin is an indication of metabolic activity, this indicated that after one week in culture >80% cultured cells showed metabolic activity.

MSCs printed in 6:2 bioink resulted in ~50% demonstrating metabolic activity, which is consistent with 6:2 bioink exhibiting relative increase in viscosity and reduced flow in the rheological studies (Figure 2C). Interestingly, printing of ECs showed metabolic activity similar to the 4:2 scaffolds (Figures 2A-D). Overall viability (metabolically active) for both MSCs in 4:2 bioink was approximately 80%, which is comparable to the viability achieved by bioinks with similar composition reported in the literature [51]. ECs showed better survival/metabolic activity in the 6:2 bioink as compared to MSCs.

3.4 Morphology of BM niche cells within scaffolds

We developed the bioinks as a platform to recapitulate the BM perivascular region. This region is important since it contains BM niche cells that facilitate cancer survival such as MSCs [52, 53]. Since we were able to maintain cell health during the bioprinting, we evaluated the morphology of two perivascular cells, MSCs and ECs within the foundational 4:2 and 6:2 scaffolds during culture.

Timeline confocal microscopy images revealed that MSCs increased in numbers in the 4:2 scaffold at days 3 and 7 (Figures 2E-G). Although there was increased number of cells in the 6:2, such enhancement was less pronounced, as compared to the same time points for the 4:2 scaffolds (Figures 2H-J). There was similar increase for EC in the 4:2 scaffolds (Figures 2K-M) but reduced cell numbers within the 6:2 scaffolds (Figures 2N-P). Furthermore, we noted little protrusion of

Preprints (www.preprints.org) | NOT PEER-REVIEWED | Posted: 7 December 2020 doi:10.20944/preprints202012.0157.v1

actin filaments, based on evaluation of cells labeled with rhodamine phalloidin, suggesting tight adherence between the cells and the hydrogel structure (Figures 2E-P). In total, MSCs and ECs survived and proliferated within the 4:2 and 6:2 scaffolds.

3.5 Ultrastructure of scaffold - comparison with BM structure

The data in Figure 1 showed similarities between the 4:2 bioinks and the mechanical properties of the marrow. Since we planned to study cancer cell behavior at the perivascular region and showed the survival of two major niche cells (Figure 2), we further analyzed the 4:2 and 6:2 bioinks for ultrastructural similarities with BM architecture. We subjected the scaffolds to scanning electron microscopy (SEM). At 72 h after printing, the images of both scaffolds revealed an ultrastructure comprised of a fibrous network with a large degree of heterogeneity (Figures 3A and 3B). However, the 4:2 scaffolds exhibited a more open structure with larger pores than the 6:2 scaffolds, which showed overall relatively condensed structure (Figures 3A and 3B). Furthermore, comparison of SEM images to previously reported images of human BM tissue uncovered striking similarities between 4:2 scaffolds and BM in terms of gross architecture, suggesting that 4:2 bioink may more closely mimic the structural organization of native BM [54, 55].

The oxygen content varies within the BM cavity [56]. We therefore investigated how the oxygen availability within the scaffold ultrastructure affected the cells embedded in 4:2 and 6:2 scaffolds. To address this question, we used the Lox1 fluorescent hypoxia probe. Image analyses identified cells in hypoxic conditions in both scaffolds, although there was ~50% less hypoxic cells in the 4:2 scaffolds as compared to the 6:2 scaffolds (Figures 3C and 3D). Interestingly, we noted a hypoxic region in the core area of the 4:2 scaffold, which contrasted in the 6:2 scaffold with a relatively homogenous curve (Figure 3E). These observations were validated by quantitative analyses with significantly ($p<0.05$) more hypoxic cells in the 6:2 scaffolds as compared to 4:2

Preprints (www.preprints.org) | NOT PEER-REVIEWED | Posted: 7 December 2020 doi:10.20944/preprints202012.0157.v1

scaffolds (Figure 3F). These results are consistent with the different pore size shown in the SEM analyses (Figures 3A and 3B). Together, the data indicate varied oxygen levels between 4:2 and 6:2 scaffolds with the latter showed continuous hypoxia across the structure.

3.6 Timeline stability of cultured scaffold

Functional studies may require long-term cultures, e.g., studies to assess hematopoietic stem cells require >6 wk cultures [57]. Therefore, to gauge the utility of 4:2 and 6:2 scaffolds for models associated with bone marrow functions, it was important to conduct analyses evaluating the stability of these scaffolds for long-term cultures. We cultured the scaffolds in DMEM with varying concentrations of FBS (0%, 2%, and 10%). We selected DMEM because it is widely utilized cell culture media for primary cell cultures. Control cultures contained deionized water or PBS, with or without Ca^{2+} and Mg^{2+}.

Weekly images of the 4:2 and 6:2 scaffolds revealed that scaffolds remained largely intact over 12 weeks (Figures 4A-B, S1, S2). However, MC and alginate crosslinks may degrade over time due to physical and ionic nature, respectively [41, 58-60]. We therefore sought to monitor the stability of these scaffold components during the culture. To achieve this, we assessed weekly concentrations of MC and Ca^{2+} (from Ca^{2+}-mediated alginate crosslinks) in the culture solution (Figures 4C-J, S3-S6). The highest concentrations of MC and Ca^{2+} from 4:2 and 6:2 scaffolds were consistently measured in the first 2 weeks of culture with 10% DMEM and dH_2O (Figures 4C-J). After this period, the concentrations decreased and remained at undetectable levels throughout the remainder the culture period. However, there was slight fluctuation in MC release when the 4:2 and 6:2 scaffolds were placed in 10% DMEM relative to increased release in deionized water (Figures 4C-J). The relatively high levels of MC and alginate crosslink breakage in the 4:2 and 6:2 scaffolds during the first 2 weeks did not significantly affect scaffold integrity based on weight

Preprints (www.preprints.org) | NOT PEER-REVIEWED | Posted: 7 December 2020 doi:10.20944/preprints202012.0157.v1

changes, which did not exceed ± 20% initial weight (Figures S7 and S8). Altogether, the data indicated stability of 4:2 and 6:2 scaffolds in common culture conditions, reinforcing their utility for long-term BM modeling applications.

3.7 Breast cancer (BC) cell behavior in the 3D scaffold

The data thus far indicated that the 4:2 bioink more closely reflects the properties of native BM tissue as compared to the 6:2 bioink. Since BC cells show preference for the BM [22, 23, 39, 43, 52, 61-66], we sought to investigate how BC cells behave in the 4:2 scaffolds. One mechanism through which BC cells evade treatment and survive for long periods in the BM is by entering into dormancy. Once of the hallmarks of identifying dormancy is increased expression of stem cell genes [43]. Therefore, we sought to determine whether such transition of BC cells could be recapitulated in the 3D bioprinted BM model.

MDA-MB-231 triple-negative BC cells with stable pOct4a-GFP was used to demarcate different subsets of cancer cells [43]. GFP intensity is a surrogate of *Oct4a* gene expression. We sorted the MDA-MB-231 based on GFP intensity and designated them as low, medium, and high Oct4a expression. We previously reported on the population with the highest GFP intensity contained drug resistant cancer stem cells that could become dormant [43].

We performed a timeline imaging of the cells for GFP in culture. After 7 days, 4:2 scaffolds seeded with high and medium GFP intensities showed little change with respect to the cell numbers (Figures 5A-B, D-E). However, the scaffolds seeded with low GFP showed an increase in cells with GFP by day 7 (Figures 5G and 5H). After 28 days, there were increases in GFP in all groups (Figures 5C, F, I). More importantly, we noted clusters of BC cells at day 28 with initiating printing of non-cancer stem cells (Oct4a low and medium), shown in blue (DAPI) clusters. Since the initial plated cells were GFP-negative, the GFP cells at day 28 strongly suggested that the 3D scaffold

 doi:10.20944/preprints202012.0157.v1

induced cell dedifferentiation. Since no other BM cells were in the culture, this indicated cell autonomous method of dedifferentiation. In summary, by culturing metastatic cancer cells in BM biomimetic scaffolds, we were able to enrich the cancer stem cell-like cells, replicating an important aspect of cancer dormancy in BM.

Preprints (www.preprints.org) | NOT PEER-REVIEWED | Posted: 7 December 2020 doi:10.20944/preprints202012.0157.v1

3.8 Figures

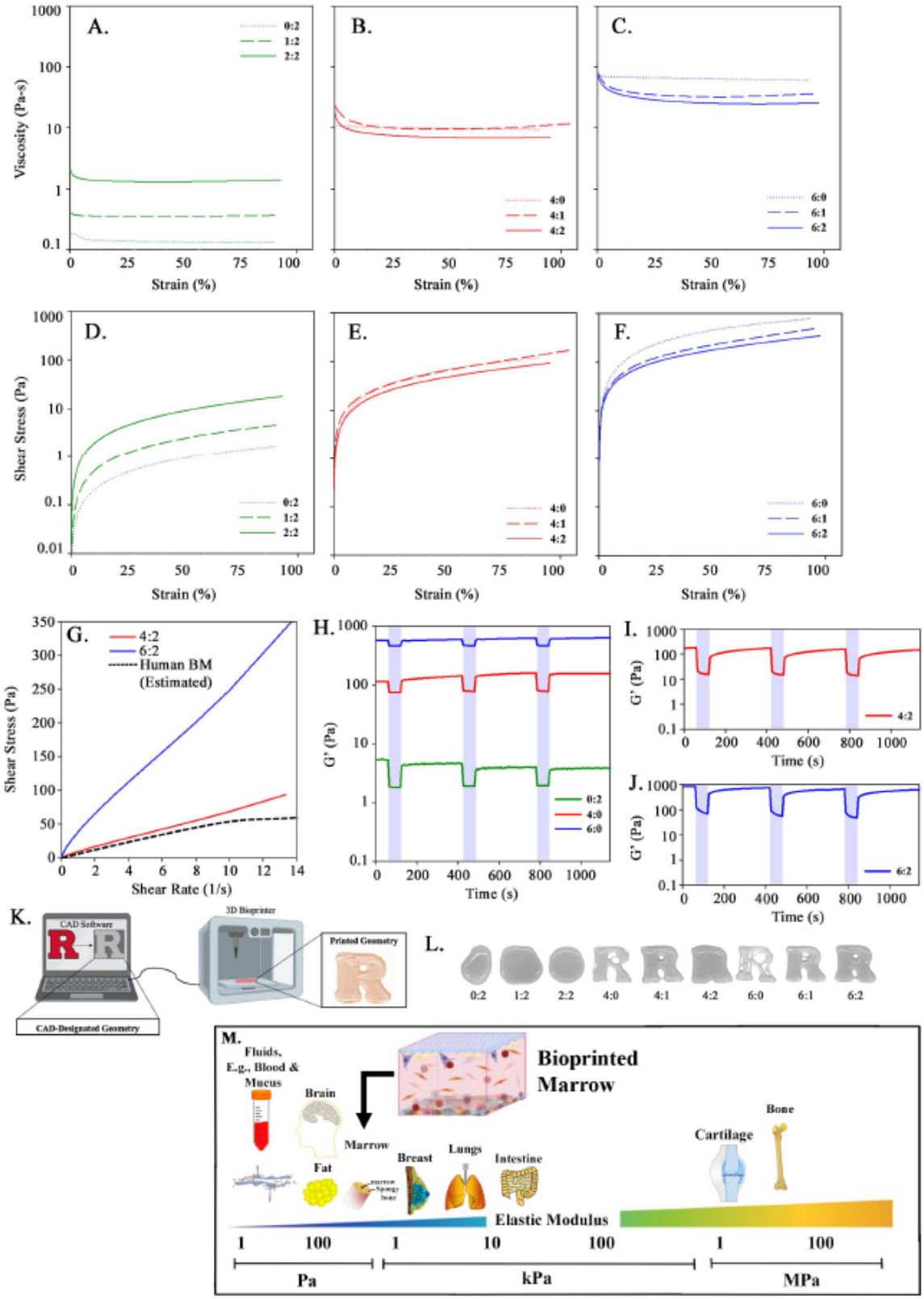

 doi:10.20944/preprints202012.0157.v1

Figure 1. Rheological analyses of hydrogels. Strain sweeps were performed using oscillatory rheometry to measure viscosity (A-C) and flow (D-F) behaviors of hydrogels containing 0-2% (w/v) MC (green), 4% MC (red), and 6% MC (blue). (G) Flow curves for 4:2 (red) and 6:2 (blue) bioinks were compared to that of human BM from a 44 year old male reported by Sobotková [15]. Shear recovery analyses for (H) single component bioinks, (I) 4:2 bioink, and (J) 6:2 bioink. (K) Shape fidelity refers to the ability of a hydrogel to maintain the designated geometry once it is printed. (L) Assessment of shape fidelity of bioinks with printing of Rutgers University logo and assessing the gross degree to which the structures resembled the designated geometry. (M) Diagrammatic summary of the spectrum of elastic moduli (G') of various bodily tissues and biomaterials as reported across the literature. Shown is femur, between 100 Pa and 100 kPa. The marrow is shown below 1 kPa, which is consistent with the perivascular and central niches.

Preprints (www.preprints.org) | NOT PEER-REVIEWED | Posted: 7 December 2020 doi:10.20944/preprints202012.0157.v1

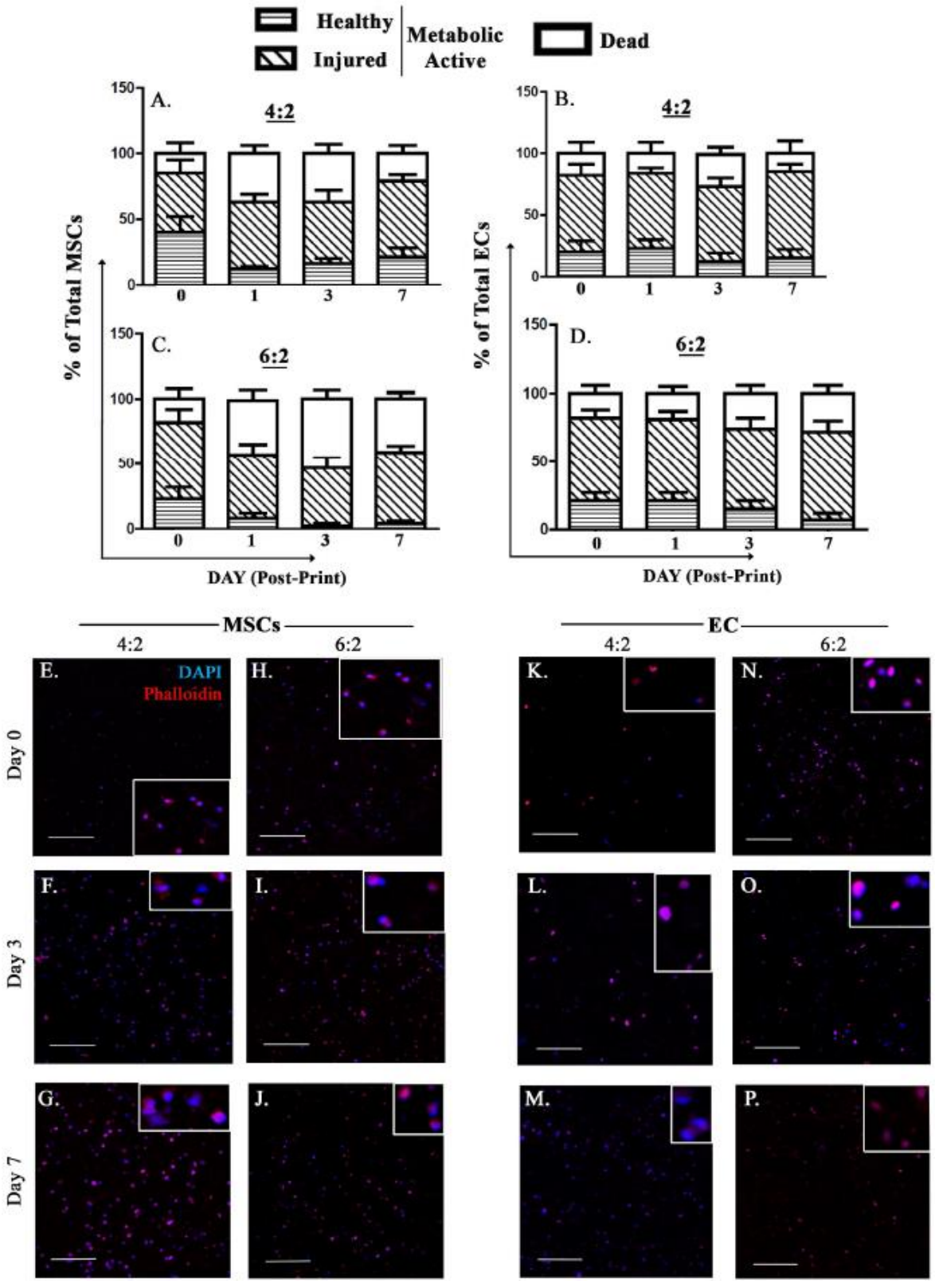

Figure 2. Cell viability and vitality are maintained by 4:2 and 6:2 bioinks. Primary human BM

 doi:10.20944/preprints202012.0157.v1

MSCs and ECs were printed into 4:2 (A, B) and 6:2 (C, D) scaffolds, respectively. Cell viability and vitality were assessed at different times up to day 7, using LIVE/DEAD Cell Vitality Assay Kit. Healthy and injured cells are viable. The analyses represent 4 independent experiments, each with a different donor. Confocal microscopy at days 1, 3 and 7 within the scaffolds: MSCs in 4:2 (E-G) and 6:2 (H-J); ECs in 4:2 (K-M) and 6:2 (N-P). Representative images at 10X magnification shown. Blue: DAPI (nuclei). Red: rhodamine phalloidin (actin). Scale bar: 250 µm.

Preprints (www.preprints.org) | NOT PEER-REVIEWED | Posted: 7 December 2020 doi:10.20944/preprints202012.0157.v1

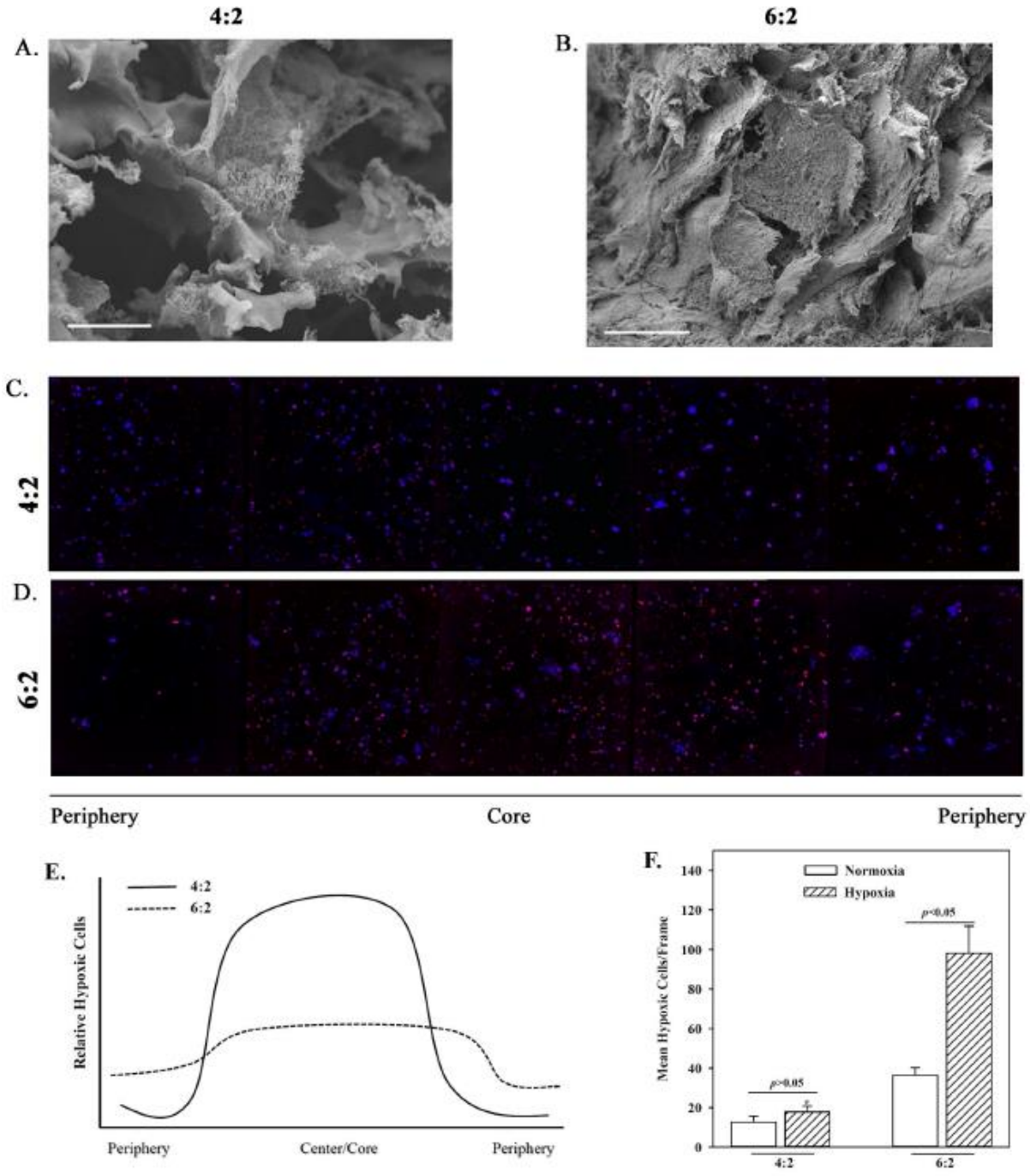

Figure 3. Scaffold ultrastructure and cell hypoxia. The ultrastructure of (A) 4:2 and (B) 6:2 cell-free scaffolds, by scanning electron microscopy (SEM). Shown are representative images at 2500X magnification. Scale bar: 10 µm. (C) Cells in 4:2 (C) and 6:2 (D) scaffolds were visualized by confocal microscopy for hypoxic cells from periphery to core. The number of hypoxic cells

 doi:10.20944/preprints202012.0157.v1

(expressing the Lox1 fluorescent hypoxia probe) in normoxic (open bar) or hypoxic (diagonal-stripped bar) incubation systems. Cells within (C) 4:2 and (D) 6:2 scaffolds treated with a Lox1 fluorescent hypoxia probe were imaged using confocal microscopy at 10X magnification. The relative differences between 'C' and 'D' along the structures are diagrammatically presented in E. The number of normoxic and hypoxic cells were counted across 5 frames and the values presented as mean cells±SD (F), * p <0.05 vs. 6:2 hypoxic cells. The images represent three different independent experiments.

Preprints (www.preprints.org) | NOT PEER-REVIEWED | Posted: 7 December 2020 doi:10.20944/preprints202012.0157.v1

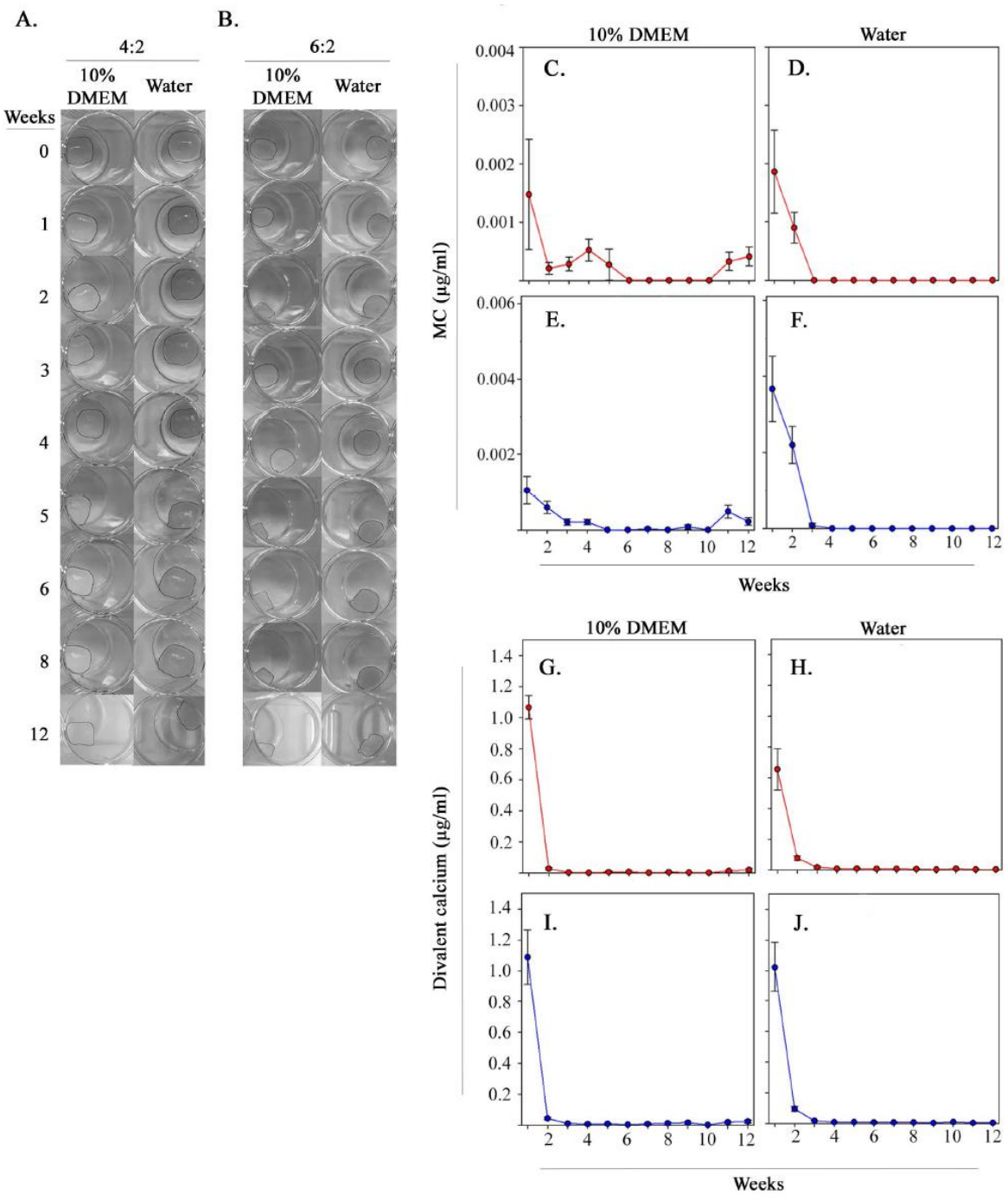

Figure 4. Stability of scaffold components in long-term culture conditions. Photographic images of (A) 4:2 and (B) 6:2 scaffolds were taken weekly for 12 weeks in 10% DMEM and deionized water, showing little bulk degradation of scaffold structure. MC (C-F) and calcium (G-

 doi:10.20944/preprints202012.0157.v1

J) concentrations in solution were measured weekly over 12 weeks for both 4:2 and 6:2 scaffolds to assess crosslink breakage over the culture period.

Preprints (www.preprints.org) | NOT PEER-REVIEWED | Posted: 7 December 2020 doi:10.20944/preprints202012.0157.v1

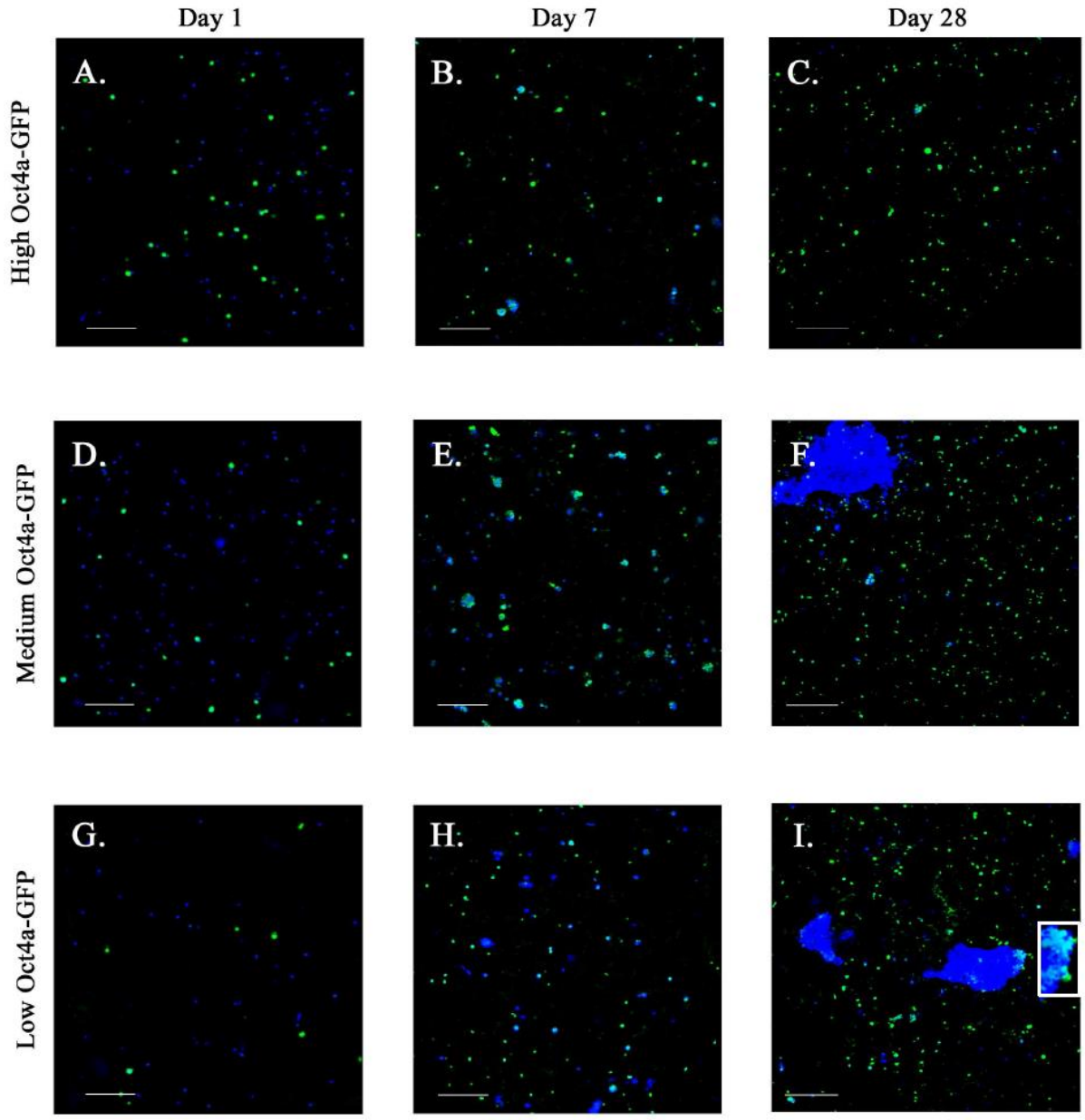

Figure 5. Bioprinting BC cell subsets in 4:2 scaffolds. MDA-MB-231 breast cancer cells (BCCs) were sorted (A-C) as Oct4a GFP-high (cancer stem cell, CSC), (D-F) GFP-medium, and (G-I) GFP-low cells. The three subsets were printed into 4:2 scaffolds. Confocal images of fixed scaffolds were acquired at days 1 (A, D, G), 7 (B, E, H), and 28 (C, F, I). Representative images at 10X magnification are shown (n=3 with 4 technical replicates). Blue: DAPI (nuclei). Green: GFP (Oct4a). Scale bar: 250 µm.

Preprints (www.preprints.org) | NOT PEER-REVIEWED | Posted: 7 December 2020 doi:10.20944/preprints202012.0157.v1

4. Discussion

3D bioprinting has revolutionized the manner to create 3D *in vitro* culture systems, allowing for rapid fabrication of constructs with pre-defined geometries. However, despite its success in creating a wide array of tissues *in silico* (e.g., breast, brain, lung, bladder), faithfully replicating very soft tissues through 3D bioprinting has proven difficult due to their limited printability and low fidelity [67-77]. This is a significant obstacle because the degree of control over the composition, size, and structure of 3D bioprinted scaffolds can meaningfully influence physiological and pathological models, including screening for drug performance. In light of this, it is not surprising that relatively little has been reported regarding biomaterials designed to specifically recapitulate the distinct physiochemical and cellular characteristics of BM, a semi-solid tissue with an elastic modulus as low as 250 Pa and a viscosity ranging from 0.04 and 125 Pa-s [15, 17, 47, 48, 78, 79].

MC-alginate composite hydrogels are emerging for extrusion bioprinting applications due to their ability to improve shape fidelity and shear thinning of bioinks [51]. We report on the development of a scaffold with MC and alginate. The intent is to establish a structure that recapitulates BM microenvironment; particularly, the perivascular region that captures events at the interface between the periphery and marrow cavity. We selected MC due to its success in maintaining hematopoietic cells and then added alginate to maintain a structure for 3D bioprinting.

Among the formulations studies, we selected 4% (w/v) MC and 2% (w/v) alginate (4:2) due to the close similarity to BM structure (Figures 1G and 3). In addition, these two formulations, in particular the 4:2 sustained printed primary human MSCs and ECs (Figure 2). Interestingly, the 4:2 structure showed a curved pattern of hypoxia, which closely mimics the BM cavity [80].

 doi:10.20944/preprints202012.0157.v1

The selection of 4:2 MC:alignate scaffold to create 3D bioprinting of BM structures is based on the following observations: i) the bioink mimics the rheological and gross ultrastructural characteristics of BM (Figures 1 and 3); ii) the bioink shows no significant negative impact cell viability and vitality, and iii) the scaffolds maintain stability in long-term culture. Furthermore, although the shape fidelity achieved using 4:2 bioink alone may not be suitable for creating large-scale or complex geometries, printing 4:2 bioink alongside a more rigid acellular "support" bioink would likely improve shape fidelity and facilitate the development of increasingly intricate structures.

Despite the absence of attached adhesion molecules, the behavior of breast cancer cells within scaffolds indicate that they are good models to study cancer metastasis. We observed clustered breast cancer cells over time in the scaffold (Figure 5). The Oct4a-hi population, which are mostly cancer stem cells [43] remained as single cells at Day 28 but retained stemness based on bright GFP (Figure 5C). This pattern was consistent with Oct4a-hi breast cancer cells being able to adapt single cell dormancy in the BM [43]. Although the seeded Oct4a-med and –lo populations were dim for GFP, over time, they gained brighter GFP and formed cell clusters, which is consistent with metastatic lesion (Figures 5F and 5I). Since the cells showed no evidence of spreading, increased cell numbers as clusters suggested that the cells might secrete extracellular matrix that provided them with a basement to survive (Figure 5).

We concluded that Oct4a-lo breast cancer cells, which began as cells with no evidence of stemness, dedifferentiate into immature functional cells. Indeed, we showed dedifferentiation of Oct4a-lo breast cancer cells when exposed to MSC exosomes (manuscript in revision). However, the 3D scaffold did not contain BM accessory cells, indicating that dedifferentiation include cell autonomous processes. This was an interesting finding because cells in 2D showed no evidence of

 doi:10.20944/preprints202012.0157.v1

cell autonomous dedifferentiation. These findings indicate the importance of the model to discern how cancer cells survive as drug resistant cells in the BM, and to study cell autonomous mechanism of BM metastasis. The development of described bioink is highly significant with respect to breast cancer studies because BM is the preferred site for this and other cancer, which leads to poor prognosis [62, 64-66, 81-83].

We evaluated mechanical similarity between bioinks (4:2 and 6:2) and endogenous BM, based on widely ranging viscosity and modulus data in the literature [15, 17, 47-49]. Variations in reported measurements may be attributable to inconsistencies in experimental approaches, such as the use of different model systems (e.g. human, bovine, porcine), sample freshness and storage method, cellular composition of samples, temperature at the time of measurements, and rheometer setup. Indeed, viscosity decreases with both temperature and shear rate, and is dependent on skeletal site [17, 46].

The described biomaterial and model are foundational and translatable with modified parameters according to the desired research application and question. For example, alginate is particularly well known in tissue engineering to exhibit poor adhesion due to a combination of lack of mammalian cell receptors for alginate and low protein adsorption to alginate gels [37]. Therefore, this allows alginate to serve as the backbone to integrate specific cell adhesion molecules, such as coupling of RGD sequences to alginate before fabricating the bioink. Indeed, the results are in line with the extensive use of these materials for cell encapsulation applications [33, 37, 51]. We printed cells sparsely at a density of 10^6 cells/ml bioink. Increased cells can be printed in the bioink to allow for intercellular interaction. Similarly, the bioink structures can incorporate supplements with soluble factors such as cytokines and insoluble factors, e.g., extracellular vesicles in cultures.

 doi:10.20944/preprints202012.0157.v1

A major application for the bioink is to print cells of the hematopoietic microenvironment. This will allow the model to serve as a platform as low-cost in drug screening. Additionally, the scaffolds containing cells could evaluate drug targeting of cancer cells in different regions within BM. This could be done together with toxicity studies; specifically, to ensure cancer target but to protect hematopoietic stem cell toxicity. Indeed, we intentionally selected the MC base to allow healthy hematopoietic cells to survive.

We did not find an overt issue with hypoxia with respect to EC and MSC viability during the first week of culture. However, oxygen availability may be significant in long-term cultures. This could be overcome with customized bioactive features, as desired by the end user, e.g., adding cell adhesion sequences or introducing soluble signaling factors.

5. Conclusion

The MC-alginate bioink reported in this study is a promising material for the development of future platforms for BM modeling. Addition of MC to low-concentration alginate enhanced printability, mimicked the rheological and ultrastructural properties of BM tissue, and supported cell viability and vitality during extrusion and subsequent cell culture. In addition, scaffolds were relatively stable and suitable for long-term cultures. Thus, this MC-alginate bioink offers a foundation for modification with bioactive factors and tissue-specific components to enhance BM mimicry. Furthermore, the expression of stem cell genes by cancer cells is a key method through which cancer cells use to survive in BM and resist treatment. We provide evidence to show 4:2 scaffolds closely replicating the structure of BM. We also showed that the structure could be applied to study breast cancer behavior in BM. We anticipate that this material can serve as a model to study the healthy microenvironment of the BM, and to uncover new methods to target elusive cancer cells and improve clinical outcomes.

Supplementary Materials: The following are available online at www.mdpi.com/xxx/s1, Table S1: Decision matrix, Figure S1: Visible degradation of 4:2 scaffolds in culture solutions, Figure S2: Visible degradation of 6:2 scaffolds in culture solutions, Figure S3: MC released from 4:2 scaffolds during long-term culture, Figure S4: MC released from 6:2 scaffolds during long-term culture. Figure S5: Alginate crosslink breakage in 4:2 scaffolds during long-term culture. Figure S6: Alginate crosslink breakage in 6:2 scaffolds during long-term culture, Figure S7: Weight fluctuation of 4:2 scaffolds during the first two weeks of culture, Figure S8: Weight fluctuation of 6:2 scaffolds during the first two weeks of culture.

Authorship Contribution:

Caitlyn A. Moore: Perform the experiments, wrote the manuscript, analyze the data, developed the concept; Zain Siddiqui: Perform the experiments, edit the manuscript; Griffin J. Carney: Perform the experiments, edit the manuscript; Yahaira Naaldijk: edited the manuscript, analyze the data, perform the experiments; Khadidiatou Guiro: edited the manuscript, analyze the data, participated in the concept; Murat Guvendiren: Edited the manuscript, participated in the concept; Vivek A. Kumar: Edited the manuscript, participated in the concept; Pranela Rameshwar: Wrote and edited the manuscript, analyze the data, develop the concepts.

Funding: This research was funded by New Jersey Commission on Cancer Research (NJCCR) for a Pre-Doctoral Fellowship to C.M.

Acknowledgements: The authors would like to acknowledge Dr. Fernando Vidal Peña and the team at the PolyRUN Facility at Rutgers-Newark for their assistance in acquiring oscillatory rheology data.

Conflicts of interest: The authors declare no conflict of interest.

References

1. J.A. DiMasi, H.G. Grabowski, R.W. Hansen, Innovation in the pharmaceutical industry: New estimates of R&D costs. *J Health Econ* **2016,** *47*, 20-33.

2. D.W. Thomas, J. Burns, J. Audette, A. Carroll, C. Dow-Hygelund, M. Hay, Clinical Development Success Rates 2006-2015. *BIO, Biomedtracker, Amplion* **2016**.

3. T.J. Hwang, D. Carpenter, J.C. Lauffenburger, B. Wang, J.M. Franklin, A.S. Kesselheim, Failure of Investigational Drugs in Late-Stage Clinical Development and Publication of Trial Results. *J Am Med Assoc* **2016,** *176* (12), 1826-1833.

4. B.M. Baker, C.S. Chen, Deconstructing the third dimension: how 3D culture microenvironments alter cellular cues. *J Cell Sci* **2012,** *125* (Pt 13), 3015-24.

5. C.M. Magin, D.L. Alge, K.S. Anseth, Bio-inspired 3D microenvironments: a new dimension in tissue engineering. *Biomed Mater* **2016,** *11* (2), 022001.

6. S.V. Murphy, A. Atala, 3D bioprinting of tissues and organs. *Nat Biotechnol* **2014,** *32* (8), 773-85.

7. K. Markstedt, A. Mantas, I. Tournier, H. Martinez Avila, D. Hagg, P. Gatenholm, 3D Bioprinting Human Chondrocytes with Nanocellulose-Alginate Bioink for Cartilage Tissue Engineering Applications. *Biomacromolecules* **2015,** *16* (5), 1489-96.

8. J.Y. Won, M.H. Lee, M.J. Kim, K.H. Min, G. Ahn, J.S. Han, S. Jin, W.S. Yun, J.H. Shim, A potential dermal substitute using decellularized dermis extracellular matrix derived bio-ink. *Artif Cells Nanomed Biotechnol* **2019,** *47* (1), 644-649.

9. R. Gaetani, P.A. Doevendans, C.H. Metz, J. Alblas, E. Messina, A. Giacomello, J.P. Sluijter, Cardiac tissue engineering using tissue printing technology and human cardiac progenitor cells. *Biomaterials* **2012,** *33* (6), 1782-90.

10. S.R. Khetani, S.N. Bhatia, Microscale culture of human liver cells for drug development. *Nat Biotechnol* **2008,** *26* (1), 120-6.

11. B. Duan, E. Kapetanovic, L.A. Hockaday, J.T. Butcher, Three-dimensional printed trileaflet valve conduits using biological hydrogels and human valve interstitial cells. *Acta Biomater* **2014,** *10* (5), 1836-46.

12. C. Fullhase, R. Soler, A. Atala, K.-E. Andersson, J.J. Yoo, A novel hybrid printing system for the generation of organized bladder tissue. *J Urol* **2009,** *181* (4), 282-283.

13. M. Tavassoli, W.H. Crosby, Bone marrow histogenesis: a comparison of fatty and red marrow. *Science* **1970,** *169* (3942), 291-3.

14. J.K. Gong, Endosteal marrow: a rich source of hematopoietic stem cells. *Science* **1978,** *199* (4336), 1443-5.

15. E. Sobotková, A. Hrubá, J. Kiefman, Z. Sobotka. *Rheological behavior of bone marrow*. Springer-Verlag Berlin: Heidelberg, 1988.

16. J.D. Bryant, T. David, P.H. Gaskell, S. King, G. Lond, Rheology of bovine bone marrow. *Proc Instn Mech Engrs* **1989,** *203*.

17. U.A. Gurkan, O. Akkus, The mechanical environment of bone marrow: a review. *Ann Biomed Eng* **2008,** *36* (12), 1978-91.

18. G.S. Travlos, Normal structure, function, and histology of the bone marrow. *Toxicol Pathol* **2006,** *34* (5), 548-65.

19. A.C. Society, Cancer Facts & Figures 2019. *Atlanta: American Cancer Society* **2019**.

20. S.M. Sarkaria, M. Decker, L. Ding, Bone Marrow Micro-Environment in Normal and Deranged Hematopoiesis: Opportunities for Regenerative Medicine and Therapies. *Bioessays* **2018,** *40* (3).

21. D.S. Krause, D.T. Scadden, A hostel for the hostile: the bone marrow niche in hematologic neoplasms. *Haematologica* **2015,** *100* (11), 1376-87.

22. P.K. Lim, S.A. Bliss, S.A. Patel, M. Taborga, M.A. Dave, L.A. Gregory, S.J. Greco, M. Bryan, P.S. Patel, P. Rameshwar, Gap junction-mediated import of microRNA from bone marrow stromal cells can elicit cell cycle quiescence in breast cancer cells. *Cancer Res* **2011,** *71* (5), 1550-60.

23. N.D. Walker, M. Elias, K. Guiro, R. Bhatia, S.J. Greco, M. Bryan, M. Gergues, O.A. Sandiford, N.M. Ponzio, S.J. Leibovich, P. Rameshwar, Exosomes from differentially activated macrophages influence dormancy or resurgence of breast cancer cells within bone marrow stroma. *Cell Death Dis* **2019,** *10* (2), 59.

24. F. Ishikawa, S. Yoshida, Y. Saito, A. Hijikata, H. Kitamura, S. Tanaka, R. Nakamura, T. Tanaka, H. Tomiyama, N. Saito, M. Fukata, T. Miyamoto, B. Lyons, K. Ohshima, N. Uchida, S. Taniguchi, O. Ohara, K. Akashi, M. Harada, L.D. Shultz, Chemotherapy-resistant human AML stem cells home to and engraft within the bone-marrow endosteal region. *Nat Biotechnol* **2007,** *25* (11), 1315-21.

25. T. Chen, G. Zhang, L. Kong, S. Xu, Y. Wang, M. Dong, Leukemia-derived exosomes induced IL-8 production in bone marrow stromal cells to protect the leukemia cells against chemotherapy. *Life Sci* **2019,** *221*, 187-195.

26. J. Wang, K. De Veirman, S. Faict, M.A. Frassanito, D. Ribatti, A. Vacca, E. Menu, Multiple myeloma exosomes establish a favourable bone marrow microenvironment with enhanced angiogenesis and immunosuppression. *J Pathol* **2016,** *239* (2), 162-73.

27. Clinical Trial Endpoints for the Approval of Cacner Drugs and Biologics: Guidance for Industry. *U. S. Dept of Health* 2018.

28. L. Shao, Y. Wang, J. Chang, Y. Luo, A. Meng, D. Zhou, Hematopoietic stem cell senescence and cancer therapy-induced long-term bone marrow injury. *Transl Cancer Res* **2013,** *2* (5), 397-411.

29. J. Hoggatt, Y. Kfoury, D.T. Scadden, Hematopoietic Stem Cell Niche in Health and Disease. *Annu Rev Pathol* **2016,** *11*, 555-81.

30. T.J. Hinton, Q. Jallerat, R.N. Palchesko, J.H. Park, M.S. Grodzicki, H.J. Shue, M.H. Ramadan, A.R. Hudson, A.W. Feinberg, Three-dimensional printing of complex biological structures by freeform reversible embedding of suspended hydrogels. *Sci Adv* **2015,** *1* (9), e1500758.

31. S. Ji, M. Guvendiren, Recent Advances in Bioink Design for 3D Bioprinting of Tissues and Organs. *Frontiers Bioeng Biotechnol* **2017,** *5* (23).

32. T. Chatterjee, A.I. Nakatani, R. Adden, M. Brackhagen, D. Redwine, H. Shen, Y. Li, T. Wilson, R.L. Sammler, Structure and properties of aqueous methylcellulose gels by small-angle neutron scattering. *Biomacromolecules* **2012,** *13* (10), 3355-69.

33. P. Nasatto, F. Pignon, J. Silveira, M. Duarte, M. Noseda, M. Rinaudo, Methylcellulose, a Cellulose Derivative with Original Physical Properties and Extended Applications. *Polymers* **2015,** *7* (5), 777-803.

34. T. Sangfai, V. Tantishaiyakul, N. Hirun, L. Li, Microphase Separation and Gelation of Methylcellulose in the Presence of Gallic Acid and NaCl as an In Situ Gel-Forming Drug Delivery System. *AAPS PharmSciTech* **2017,** *18* (3), 605-616.

35. M.K. Bain, B. Bhowmick, D. Maity, D. Mondal, M.M. Mollick, B.K. Paul, M. Bhowmik, D. Rana, D. Chattopadhyay, Effect of PVA on the gel temperature of MC and release kinetics of KT from MC based ophthalmic formulations. *Int J Biol Macromol* **2012,** *50* (3), 565-72.

36. N.N. Iscove, F. Sieber, K.H. Winterhalter, Erythroid colony formation in cultures of mouse and human bone marrow: analysis of the requirement for erythropoietin by gel filtration and affinity chromatography on agarose-concanavalin A. *J Cell Physiol* **1974,** *83* (2), 309-20.

37. K.Y. Lee, D.J. Mooney, Alginate: properties and biomedical applications. *Prog Polym Sci* **2012,** *37* (1), 106-126.

38. J. Jia, D.J. Richards, S. Pollard, Y. Tan, J. Rodriguez, R.P. Visconti, T.C. Trusk, M.J. Yost, H. Yao, R.R. Markwald, Y. Mei, Engineering alginate as bioink for bioprinting. *Acta Biomater* **2014,** *10* (10), 4323-31.

39. S.J. Greco, S.A. Patel, M. Bryan, L.F. Pliner, D. Banerjee, P. Rameshwar, AMD3100-mediated production of interleukin-1 from mesenchymal stem cells is key to chemosensitivity of breast cancer cells. *Am J Cancer Res* **2011,** *1* (6), 701-15.

40. J.A. Potian, H. Aviv, N.M. Ponzio, J.S. Harrison, P. Rameshwar, Veto-like activity of mesenchymal stem cells: functional discrimination between cellular responses to alloantigens and recall antigens. *J Immunol* **2003,** *171* (7), 3426-34.

41. K. Schutz, A.M. Placht, B. Paul, S. Bruggemeier, M. Gelinsky, A. Lode, Three-dimensional plotting of a cell-laden alginate/methylcellulose blend: towards biofabrication of tissue engineering constructs with clinically relevant dimensions. *J Tissue Eng Regen Med* **2017,** *11* (5), 1574-1587.

42. M.K. Bain, M. Bhowmik, D. Maity, N.K. Bera, S. Ghosh, D. Chattopadhyay, Control of thermo reversible gelation of methylcellulose using polyethylene glycol and sodium chloride for sustained delivery of ophthalmic drug. *J Applied Polymer Sci* **2010**, 118, 631-637.

43. S.A. Patel, S.H. Ramkissoon, M. Bryan, L.F. Pliner, G. Dontu, P.S. Patel, S. Amiri, S.R. Pine, P. Rameshwar, Delineation of breast cancer cell hierarchy identifies the subset responsible for dormancy. *Sci Rep* **2012,** *2*, 906.

44. S.A. Bliss, S. Paul, P.W. Pobiarzyn, S. Ayer, G. Sinha, S. Pant, H. Hilton, N. Sharma, M.F. Cunha, D.J. Engelberth, S.J. Greco, M. Bryan, M.J. Kucia, S.S. Kakar, M.Z. Ratajczak, P. Rameshwar, Evaluation of a developmental hierarchy for breast cancer cells to assess risk-based patient selection for targeted treatment. *Sci Rep* **2018,** *8* (1), 367.

45. A. Blaeser, D.F. Duarte Campos, U. Puster, W. Richtering, M.M. Stevens, H. Fischer, Controlling Shear Stress in 3D Bioprinting is a Key Factor to Balance Printing Resolution and Stem Cell Integrity. *Adv Healthc Mater* **2016,** *5* (3), 326-33.

46. J.D. Bryant, T. David, P.H. Gaskell, S. King, G. Lond, Rheology of bovine bone marrow. *Proc Instn Mech Engrs* **1989,** *203*, 71-75.

47. Z. Zhong, O. Akkus, Effects of age and shear rate on the rheological properties of human yellow bone marrow. *Biorheology* **2011,** *48* (2), 89-97.

48. L.E. Jansen, N.P. Birch, J.D. Schiffman, A.J. Crosby, S.R. Peyton, Mechanics of intact bone marrow. *J Mech Behav Biomed Mater* **2015,** *50*, 299-307.

49. T.A. Metzger, J.M. Shudick, R. Seekell, Y. Zhu, G.L. Niebur, Rheological behavior of fresh bone marrow and the effects of storage. *J Mech Behav Biomed Mater* **2014,** *40*, 307-313.

50. D.B. Kolesky, R.L. Truby, A.S. Gladman, T.A. Busbee, K.A. Homan, J.A. Lewis, 3D Bioprinting of Vascularized, Heterogeneous Cell-Laden Tissue Constructs. *Adv Materials* **2014,** *26* (19), 3124-3130.

51. T. Ahlfeld, V. Guduric, S. Duin, A.R. Akkineni, K. Schutz, D. Kilian, J. Emmermacher, N. Cubo-Mateo, S. Dani, M.V. Witzleben, J. Spangenberg, R. Abdelgaber, R.F. Richter, A. Lode, M. Gelinsky, Methylcellulose - a versatile printing material that enables biofabrication of tissue equivalents with high shape fidelity. *Biomater Sci* **2020,** *8* (8), 2102-2110.

52. S.A. Bliss, G. Sinha, O.A. Sandiford, L.M. Williams, D.J. Engelberth, K. Guiro, L.L. Isenalumhe, S.J. Greco, S. Ayer, M. Bryan, R. Kumar, N.M. Ponzio, P. Rameshwar, Mesenchymal Stem Cell-Derived Exosomes Stimulate Cycling Quiescence and Early Breast Cancer Dormancy in Bone Marrow. *Cancer Res* **2016,** *76* (19), 5832-5844.

53. C.M. Ghajar, H. Peinado, H. Mori, I.R. Matei, K.J. Evason, H. Brazier, D. Almeida, A. Koller, K.A. Hajjar, D.Y. Stainier, E.I. Chen, D. Lyden, M.J. Bissell, The perivascular niche regulates breast tumour dormancy. *Nat Cell Biol* **2013,** *15* (7), 807-17.

54. D. Kanthi, Simulation of the bone marrow microenvironment, Fachgebiet Medizinische Biotechnologie, Technische Universität Berlin, Berlin, 2013.

55. M.A. Lichtman, The Ultrastructure of the Hemopoietic Environment of the Marrow: A Review. *Exp Hematol* **1981,** *9* (4), 391-410.

56. T. Binzoni, T.S. Leung, C. Courvoisier, R. Giust, G. Tribillon, T. Gharbi, D.T. Delpy, Blood volume and haemoglobin oxygen content changes in human bone marrow during orthostatic stress. *J Physiol Anthropol* **2006,** *25* (1), 1-6.

57. M. Gergues, V. Nagula, S.A. Bliss, A. Eljarrah, S. Ayer, N. Gnanavel, G. Sinha, Q. Wu, G. Yehia, S.J. Greco, J. Qian, P. Rameshwar, Neuroimmune/Hematopoietic Axis with Distinct Regulation by the High-Mobility Group Box 1 in Association with Tachykinin Peptides. *J Immunol* **2020,** *204* (4), 879-891.

58. M.A. LeRoux, F. Guilak, L.A. Setton, Compressive and shear properties of alginate gel: Effects of sodium ions and alginate concentration. *J Biomed Mater Res* **1999,** *47*, 46-53.

59. C.K. Kuo, P.X. Ma, Maintaining dimensions and mechanical properties of ionically crosslinked alginate hydrogel scaffolds in vitro. *J Biomed Mater Res A* **2008,** *84* (4), 899-907.

60. K.Y. Lee, K.H. Bouhadir, D.J. Mooney, Controlled degradation of hydrogels using multi-functional cross-linking molecules. *Biomaterials* **2004,** *25* (13), 2461-6.

61. S.A. Patel, J.R. Meyer, S.J. Greco, K.E. Corcoran, M. Bryan, P. Rameshwar, Mesenchymal stem cells protect breast cancer cells through regulatory T cells: role of mesenchymal stem cell-derived TGF-beta. *J Immunol* **2010,** *184* (10), 5885-94.

62. S. Braun, F.D. Vogl, B. Naume, W. Janni, M.P. Osborne, C. Coombes, G. Schlimok, I.J. Diel, B. Gerber, G. Gebauer, J.-Y. Pierga, C. Marth, D. Oruzio, G. Wiedswang, E.-F. Solomayer, G. Kundt, B. Strobl, T. Fehm, G.Y.C. Wong, J. Bliss, A. Vincent-Salomon, K.

Pantel, A Pooled Analysis of Bone Marrow Micrometastasis in Breast Cancer. *New Eng J Med* **2005,** *353* (8), 793-802.

63. M. Ono, N. Kosaka, N. Tominaga, Y. Yoshioka, F. Takeshita, R.U. Takahashi, M. Yoshida, H. Tsuda, K. Tamura, T. Ochiya, Exosomes from bone marrow mesenchymal stem cells contain a microRNA that promotes dormancy in metastatic breast cancer cells. *Sci Signal* **2014,** *7* (332), ra63.

64. B. Naume, X. Zhao, M. Synnestvedt, E. Borgen, H.G. Russnes, O.C. Lingjaerde, M. Stromberg, G. Wiedswang, G. Kvalheim, R. Karesen, J.M. Nesland, A.L. Borresen-Dale, T. Sorlie, Presence of bone marrow micrometastasis is associated with different recurrence risk within molecular subtypes of breast cancer. *Mol Oncol* **2007,** *1* (2), 160-71.

65. S. Braun, K. Pantel, P. Muller, W. Janni, F. Hepp, C.R. Kentenich, S. Gastroph, A. Wischnik, T. Dimpfl, G. Kindermann, G. Riethmuller, G. Schlimok, Cytokeratin-positive cells in the bone marrow and survival of patients with stage I, II, or III breast cancer. N *N Engl J Med* **2000,** *342* (8), 525-33.

66. S. Braun, K. Pantel, Clinical significance of occult metastatic cells in bone marrow of breast cancer patients. *Oncologist* **2001,** *6* (2), 125-32.

67. E.P. Carter, J.A. Gopsill, J.J. Gomm, J.L. Jones, R.P. Grose, A 3D in vitro model of the human breast duct: a method to unravel myoepithelial-luminal interactions in the progression of breast cancer. *Breast Cancer Res* **2017,** *19* (1), 50.

68. P.-A. Vidi, M.J. Bissell, S.A. Lelièvre, Three-Dimensional Culture of Human Breast Epithelial Cells: The How and the Why. In *Epithelial Cell Culture Protocols*, 2012; pp 193-219.

69. J.A. Reid, P.A. Mollica, R.D. Bruno, P.C. Sachs, Consistent and reproducible cultures of large-scale 3D mammary epithelial structures using an accessible bioprinting platform. *Breast Cancer Res* **2018,** *20* (1), 122.

70. M.D. Tang-Schomer, W.B. Wu, D.L. Kaplan, M.J. Bookland, In vitro 3D regeneration-like growth of human patient brain tissue. *J Tissue Eng Regen Med* **2018,** *12* (5), 1247-1260.

71. K.M. Koss, M.A. Churchward, A.F. Jeffery, V.K. Mushahwar, A.L. Elias, K.G. Todd, Improved 3D Hydrogel Cultures of Primary Glial Cells for In Vitro Modelling of Neuroinflammation. *J Visualized Expts* **2017,** (130)56615.

72. P.K. Kabadi, A.L. Rodd, A.E. Simmons, N.J. Messier, R.H. Hurt, A.B. Kane, A novel human 3D lung microtissue model for nanoparticle-induced cell-matrix alterations. *Part Fibre Toxicol* **2019,** *16* (1), 15.

73. P.A. Link, R.A. Pouliot, N.S. Mikhaiel, B.M. Young, R.L. Heise, Tunable Hydrogels from Pulmonary Extracellular Matrix for 3D Cell Culture. *J Visualized Expts* **2017,** (119) 55094.

74. R. Bhowmick, T. Derakhshan, Y. Liang, J. Ritchey, L. Liu, H. Gappa-Fahlenkamp, A Three-Dimensional Human Tissue-Engineered Lung Model to Study Influenza A Infection. *Tissue Engineering Part A* **2018,** *24* (19-20), 1468-1480.

75. A. Shoae-Hassani, S.A. Mortazavi-Tabatabaei, S. Sharif, A.M. Seifalian, A. Azimi, A. Samadikuchaksaraei, J. Verdi, Differentiation of human endometrial stem cells into urothelial cells on a three-dimensional nanofibrous silk-collagen scaffold: an autologous cell resource for reconstruction of the urinary bladder wall. *J Tissue Eng Regen Med* **2015,** *9* (11), 1268-76.

76. H. Tian, S. Bharadwaj, Y. Liu, H. Ma, P.X. Ma, A. Atala, Y. Zhang, Myogenic differentiation of human bone marrow mesenchymal stem cells on a 3D nano fibrous scaffold for bladder tissue engineering. *Biomaterials* **2010,** *31* (5), 870-7.

77. A. Skardal, A. Atala, Biomaterials for integration with 3-D bioprinting. *Ann Biomed Eng* **2015,** *43* (3), 730-46.

78. M.R. Nelson, K. Roy, Bone-marrow mimicking biomaterial niches for studying hematopoietic stem and progenitor cells. *J Materials Chem B* **2016,** *4* (20), 3490-3503.

79. P. de la Puente, B. Muz, R.C. Gilson, F. Azab, M. Luderer, J. King, S. Achilefu, R. Vij, A.K. Azab, 3D tissue-engineered bone marrow as a novel model to study pathophysiology and drug resistance in multiple myeloma. *Biomaterials* **2015,** *73*, 70-84.

80. J.A. Spencer, F. Ferraro, E. Roussakis, A. Klein, J. Wu, J.M. Runnels, W. Zaher, L.J. Mortensen, C. Alt, R. Turcotte, R. Yusuf, D. Côté, S.A. Vinogradov, D.T. Scadden, C.P. Lin, Direct measurement of local oxygen concentration in the bone marrow of live animals. *Nature* **2014,** *508* (7495), 269-273.

81. I.J. Diel, M. Kaufmann, R. Goerner, S.D. Costa, S. Kaul, G. Bastert, Detection of tumor cells in bone marrow of patients with primary breast cancer: a prognostic factor for distant metastasis. *J Clin Oncol* **1992,** *10* (10), 1534-1539.

82. J.L. Mansi, U. Berger, T. McDonnell, A. Pople, Z. Rayter, J.C. Gazet, R.C. Coombes, The fate of bone marrow micrometastases in patients with primary breast cancer. *J Clin Oncol* **1989,** *7* (4), 445-9.

83. F.C. Bidard, A. Vincent-Salomon, B. Sigal-Zafrani, M. Rodrigues, V. Dieras, L. Mignot, X. Sastre-Garau, M.F. Poupon, J.Y. Pierga, Time to metastatic relapse and breast cancer cells dissemination in bone marrow at metastatic relapse. *Clin Exp Metastasis* **2008,** *25* (8), 871-5.